

Nightjar: Dynamic Adaptive Speculative Decoding for Large Language Models Serving

Rui Li, Zhaoning Zhang, Libo Zhang, Huaimin Wang, Xiang Fu, Zhiquan Lai
State Key Laboratory of Complex & Critical Software Environment
National Key Laboratory of Parallel and Distributed Computing
College of Computer Science and Technology, National University of Defense Technology
Changsha, China

Abstract—Speculative decoding (SD) accelerates LLM inference by verifying draft tokens in parallel. However, this method presents a critical trade-off: it improves throughput in low-load, memory-bound systems but degrades performance in high-load, compute-bound environments due to verification overhead. Existing Speculative Decoding strategies typically rely on static speculative lengths, failing to adapt to fluctuating request loads or identify the optimal moment to halt speculation. The cost of restarting speculative inference also remains unquantified. During traffic surges, the marginal utility of speculation diminishes; yet, the draft model’s persistent memory footprint competes for available KV cache. This resource contention limits the maximum batch size, thereby degrading overall system throughput. To overcome this, we propose Nightjar, a novel learning-based algorithm for adaptive speculative inference that adjusts to request load by dynamically selecting the optimal speculative length for different batch sizes. Upon detecting significant request queuing and KV cache shortages, we disable speculative decoding and offload the draft model to the CPU. This reclaims VRAM for the KV cache, thereby facilitating larger batch sizes and maximizing overall system throughput. Experiments show that Nightjar achieves up to 14.8% higher throughput and 20.2% lower latency compared to standard speculative decoding, demonstrating robust efficiency for real-time serving.

Index Terms—Speculative decoding, Large language models serving, Multi-armed bandit, Dynamic real-time request loads

1. Introduction

Large language models (LLMs) are increasingly deployed in real-world applications, where they serve concurrent requests with varying throughput requirements. However, the LLM serving system faces high latency and low throughput due to the sequential nature of autoregressive decoding and the limited memory of the GPU [1].

Speculative decoding (SD) [2], [3] accelerates inference by allowing a draft model to propose multiple candidate

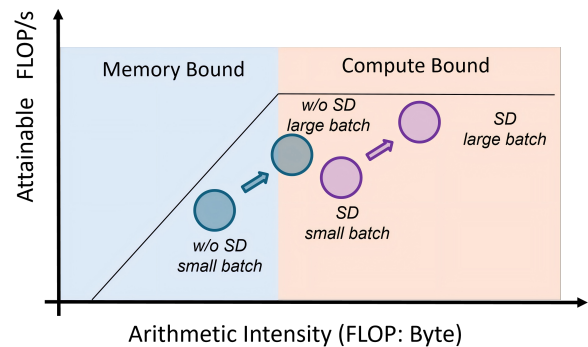


Figure 1. Schematic roofline illustration of autoregressive decoding (w/o SD) and speculative decoding (SD); positions are illustrative.

tokens, while the target model verifies them in parallel, which is theoretically lossless in terms of accuracy. This reduces the strictly sequential dependency in autoregressive decoding and increases concurrency. From a roofline perspective (Figure 1), under small batch sizes, speculative decoding raises arithmetic intensity by verifying multiple draft tokens per weight, enhancing utilization in the memory-bound regime. As batch size increases, compute demands dominate and the speculative verification overhead pushes the system into the larger compute-bound region, diminishing speculative gains, whereas traditional autoregressive decoding scales more efficiently and increases throughput.

However, current speculative decoding implementations (e.g., in vLLM [4]) often use a fixed speculative length, which is not optimal for dynamic request loads. The optimal speculative length is a dynamic variable dictated by the interplay of batch size, token acceptance rates, and hardware characteristics. An excessively long speculative length increases the time spent on draft generation and imposes significant verification overhead, whereas a length that is too short fails to fully capitalize on the potential speedup of speculative decoding.

Furthermore, model-based draft models consume both compute resources and precious GPU memory (VRAM), unlike model-free approaches such as N-gram that incur negligible memory footprints. However, model-free methods

lack generalizability and are often restricted to specific domains like code generation [5]. In high-traffic scenarios, the VRAM occupied by these draft models directly competes with the KV cache; reclaiming this space for the KV cache would facilitate larger batch sizes and significantly maximize overall system throughput.

Most optimizations for speculative decoding ignore the volatility of real-world serving. Early works targeted single requests [6], [7], [8], [9], [10] or static batches [11], [12], making them unsuitable for fluctuating traffic. Newer dynamic approaches [11], [13], [14], [15] also have flaws. For example, SpecServe [14] and TETRIS [16] rely on draft confidence, which scales poorly with large batch sizes. DSD [13] adjusts length based on historical acceptance rates. This creates a ‘deadlock’: if speculation is turned off, data collection stops, trapping the system in a suboptimal state. Even BanditSpec [12], which introduced Multi-Armed Bandits, uses a static design that is incompatible with the continuous batching of modern systems.

While existing works such as Oneiros [17] and eLLM [18] attempt to optimize GPU memory through memory remapping or shared pools, they predominantly focus on general-purpose memory management within or across models. Consequently, they overlook the tight coupling between strategic policy decisions (e.g., speculative length) and memory allocation (e.g., the residency of the draft model) inherent in the speculative decoding paradigm.

Therefore, the field urgently needs a truly intelligent, adaptive decision-making mechanism that can perceive load changes in real-time and accurately weigh the trade-offs between benefits and costs. It must be capable of dynamically selecting the optimal speculative strategy for different batch sizes at each decoding step—including decisively disabling it when necessary. To address this core challenge, we propose **Nightjar**, a contextual bandit approach for speculative length selection in dynamic, real-time LLM services. A key feature of our approach is its ability to learn the optimal speculative length for different batch sizes at each decoding step, without requiring prior knowledge of request difficulty or model characteristics. Furthermore, we incorporate the switching cost of transitioning from a speculative length of 0 to a positive value, a factor previously overlooked. By dynamically offloading the draft model upon disabling speculative inference, we reclaim substantial VRAM for the KV cache, thereby facilitating larger batch sizes and maximizing overall system throughput. Simultaneously, when a reduction in request load is detected, we proactively and asynchronously reload the draft model to re-enable speculative decoding, ensuring sustained performance gains. Implemented on vLLM [4] and evaluated on three real-world datasets, Nightjar consistently outperforms existing methods, achieving up to 14.8% higher throughput and 20.2% lower latency compared to standard speculative decoding, demonstrating its practical effectiveness for real-time LLM serving.

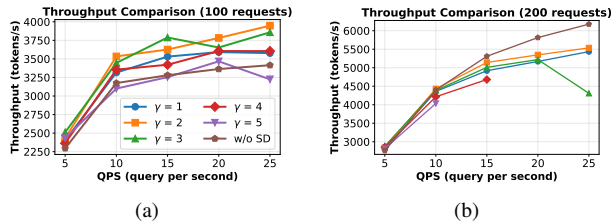


Figure 2. Throughput under different request loads and rates. γ denotes the speculative length (tokens generated by the draft model per step). Note: Configurations with $\gamma \geq 4$ are omitted at high QPS due to GPU out-of-memory (OOM) errors.

2. Motivation

Although modern LLM serving systems, e.g., vLLM [4], have been widely adopted in production, challenges remain in achieving high throughput and low latency with speculative decoding.

2.1. Dynamic Speculative Decoding Length Selection

In speculative decoding, the draft model generates γ tokens, which are subsequently verified by the target model in parallel. Consequently, the total latency per iteration is the sum of the draft model’s generation time and the target model’s verification time. The actual number of tokens produced per step equals the number of accepted tokens (n) plus one bonus token. While increasing the speculative length γ can potentially raise the number of accepted tokens, it also incurs a higher temporal cost. If the acceptance rate (the ratio of accepted tokens to γ) is low, the added overhead may outweigh the gains, ultimately leading to a decrease in overall throughput.

We empirically validate this trade-off¹. As shown in Figure 2(a), SD provides significant speedups at lower request loads. For instance, a speculative length (γ) of 3 improves throughput by 15.5% at 15 QPS while a speculative length of 2 yields better improvement than 3 at QPS=25. However, as the load increases, Autoregressive (AR) decoding surpasses SD’s performance. At high loads (Figure 2(b)), the overhead becomes detrimental, leading to a performance degradation of up to 30.25% compared to AR. This confirms that SD excels in the memory-bound regime, while its verification overhead becomes a liability when the system is compute-bound.

The core challenge lies in the dynamic and unpredictable nature of real-world LLM serving loads. Consequently, a fixed speculative length is inherently suboptimal, as a configuration tuned for low-load efficiency can degrade service under high traffic. The optimal speculative length is not a static value but a dynamic variable dependent on real-time

1. Experiments were conducted on the ShareGPT dataset using vLLM with the DeepSeek-R1-Distill-Qwen-7B model and a 0.5B draft model [19] on an RTX 4090 GPU.

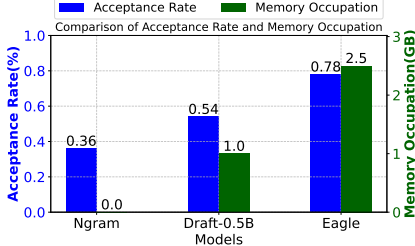


Figure 3. Memory occupation for different draft methods.

factors like system load, hardware characteristics, and token acceptance rates [20].

2.2. Memory underutilization

TABLE 1. KV CACHE MEMORY OCCUPATION FOR DIFFERENT MODELS.

Context Length	Vicuna-13B (MHA)	DeepSeek-R1-Distill-Qwen-7B
1,024 (1K)	800 MiB	56 MiB
4,096 (4K)	3,200 MiB (3.12 GiB)	224 MiB
8,192 (8K)	6,400 MiB (6.25 GiB)	448 MiB
32,768 (32K)	25,600 MiB (25.00 GiB)	1,792 MiB (1.75 GiB)

As evidenced by Table 1, the memory footprint of the KV cache is not only substantial but scales aggressively with context length, transitioning from a negligible overhead to a primary consumer of GPU resources. This expansion creates a zero-sum competition within the finite VRAM budget: as the KV cache encroaches upon the available memory, it directly constrains the headroom for resident draft model weights. Such resource contention highlights a critical bottleneck in static memory partitioning, where the burgeoning cache demands can eventually marginalize auxiliary models and degrade overall system throughput.

As shown in Figure 3, draft models (Ngram, DeepSeek-R1-DRAFT-Qwen2.5-0.5B [19]) occupy varying GPU memory, impacting KV cache capacity. While their weights are smaller than the main model, they constrain memory under high loads. For instance, unloading a 1.4GB draft model (e.g., 14B Multi-Token Prediction (MTP) for DeepSeek 671B [21]) frees space for 49k additional tokens in KV cache (calculated via MLA [21]). Current systems (e.g., vLLM [4]) retain draft models even when SD is disabled, wasting memory.

We identify that memory inefficiency arises from the isolation of weight and KV cache spaces in existing systems. This isolation hinders the dynamic redistribution of memory resources based on workload demands, leading to underutilized activation memory, which exacerbates KV cache space pressure and ultimately constrains overall system performance.

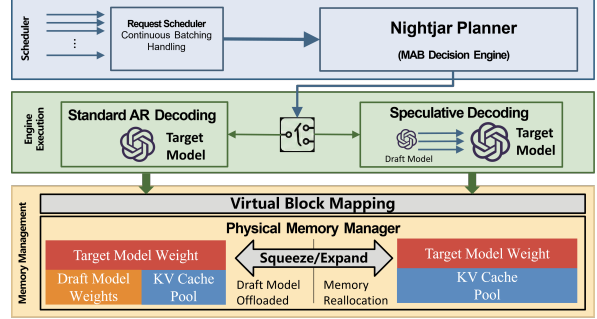


Figure 4. An overview of our adaptive approach with multi-armed bandit (MAB) for dynamic request load.

3. Nightjar Design

In this section, we first introduce the problem statement and the key notations used in Nightjar. Then, we present the algorithm design and the elastic memory management mechanism for Speculative Decoding.

3.1. Overview

Nightjar consists of two core components: 1) **Speculative Length Selection**: A contextual multi-armed bandit (MAB) algorithm that selects the optimal speculative length for each batch size in continual batching. If the speculative length is selected to be 0, the draft model will not be used and the system will switch to the standard autoregressive decoding. Otherwise, the draft model will be used to generate the speculative length tokens, and the target model will verify them in parallel. 2) **Elastic Memory Management**: A mechanism that dynamically allocates memory for the draft model. If the draft model is not used, and request rate is high, and there is not enough GPU memory for KV cache to allocate, we free the draft model in the GPU and make room for the KV cache. When the request rate is low, we load the draft model back into the GPU to accelerate the generation, as illustrated in Figure 4.

4. Multi-Armed Bandit for Speculative Length Selection

In this section, we introduce the multi-armed bandit (MAB) for speculative length selection.

4.1. Problem Statement

In continual batching [4] for LLM serving, the batch size can vary at each decoding step. We consider batch sizes $B \in \mathcal{B} = \{1, 2, \dots, B_{\max}\}$ and speculative lengths $\gamma \in \{0, 1, \dots, \Gamma_{\max}\}$. Following [13], we evaluate performance using *goodput* $g_{B,\gamma}$, defined as the number of tokens generated per second, including both accepted proposed tokens and bonus tokens generated during verification.

Our objective is to select, for each batch size B , the speculative length γ that maximizes goodput:

$$\gamma^*(B) = \arg \max_{\gamma \in \{0, 1, \dots, \Gamma_{\max}\}} g_{B, \gamma} \quad (1)$$

However, $g_{B, \gamma}$ depends on the token acceptance rate, which is unknown a priori. We model the problem as a regret minimization task over T steps. We define the reward r_{γ}^t as the realized goodput observed after selecting arm γ at step t . The cumulative regret is:

$$R(T) = \sum_{t=1}^T \left(r_{\gamma_t^*}^t - r_{\gamma_t}^t \right) \quad (2)$$

Our goal is to find a policy that minimizes $R(T)$. We summarize the key notations and their descriptions in Table 2.

TABLE 2. SUMMARY OF KEY NOTATIONS USED IN NIGHTJAR.

Symbol	Description
<i>System Parameters & Cost Model</i>	
B, B_{\max}	Current and maximum batch size, where $B \in \{1, \dots, B_{\max}\}$.
γ, Γ_{\max}	Current and maximum speculative length (draft tokens).
c_{prefill}	Latency overhead for reconstructing the KV cache (switching cost).
L_{\max}	Effective skip length, defined as $\max_{i \in B} L_i$ (max lag in a batch).
C_{switch}	Upper bound constant for the switching cost.
<i>Elastic Memory Management</i>	
$M_{\text{orig}}, M_{\text{scale}}$	Baseline KV cache capacity and expanded capacity after offloading.
S_{draft}	Memory footprint required to store the draft model weights.
N_{free}	Number of currently available physical KV cache blocks.
τ_{low}	Critical scarcity threshold triggering memory expansion.
T_{persist}	Temporal window size for validating low-memory states.
$ Q_{\text{wait}} $	Cardinality of the request waiting queue.
<i>MAB Hierarchical Structure</i>	
t	Global decoding time step index.
j_B	Block index for batch size B , governing long-term scheduling scales.
b_B	Bin index within block j_B , controlling exploration probability ($p \propto 1/\sqrt{b_B}$).
τ_B	Round counter within bin b_B .
H_B	Duration of the current block, growing exponentially as 2^{j_B-1} .
<i>Performance Metrics & Regret Analysis</i>	
$g_{B, \gamma}, \tilde{g}_{B, \gamma}$	Theoretical goodput and its empirical mean estimate.
γ_t^*	Optimal speculative length at time t that minimizes the objective.
$r_t(\gamma)$	Realized reward (observed goodput) at step t for arm γ .
$N_t(\gamma)$	Number of times arm γ has been selected up to time t .
$\beta_t(\gamma)$	Confidence radius for the goodput estimate at time t .
$R(T)$	Cumulative regret over horizon T relative to the optimal policy.
δ	Confidence parameter, where estimates hold with prob. $1 - \delta$.

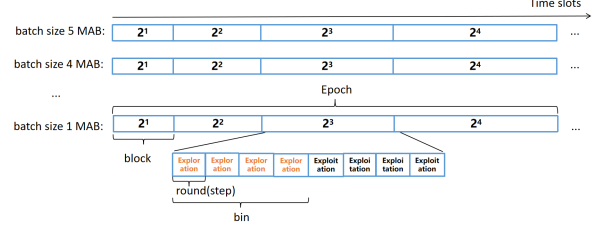


Figure 5. Illustration of the Nightjar algorithm’s three-level hierarchy. Each batch size maintains its own **Epoch**. Each epoch contains **Blocks** (j_B) of exponentially growing duration, which are responsible for the long-term schedule. These blocks are further divided into fixed-size **Bins** (b_B), the basic units for controlling the exploration-exploitation trade-off. Each **round** (τ_B) is a decoding step.

4.2. Algorithm Design

Contextual MAB can take dynamic request batch size or input sequences as context, such as linear Thompson [22], LinUCB [23], which have been successfully applied in online prediction settings such as configuration selection [24]. However, they are questionable in dynamic serving environments. We adopt the relatively simple framework ADA-BINGREEDY proposed in [25]. One difference between [25] and our approach is that we develop a request batch mechanism to handle varying request patterns. And we design reward that considers the speculative length switch cost.

As shown in Figure 5, the Nightjar algorithm adaptively selects the speculative length γ for each batch under continuous batching by organizing time into blocks and bins to balance exploration and exploitation.

The decision-making process in Nightjar is driven by an objective function that minimizes the inverse goodput while penalizing frequent re-initializations of the draft model. Formally, at global time t with batch size B , the optimal speculative length γ_t^* for an exploitation step is determined by:

$$\gamma_t^* = \arg \min_{\gamma \in \{0, 1, \dots, \Gamma_{\max}\}} \left\{ \frac{1}{\tilde{g}_{B, \gamma}} + \frac{\mathbb{I}(\gamma_{t-1} = 0 \wedge \gamma > 0) \cdot c_{\text{prefill}}}{\gamma} \right\} \quad (3)$$

Here, we estimate the empirical mean goodput $\tilde{g}_{B, \gamma}$ using an incremental cumulative moving average to ensure computational efficiency without storing historical reward sequences. Upon observing a new reward r_t for a specific batch size B and speculative length γ at the n -th visit, the statistic is updated iteratively via $\tilde{g}_{B, \gamma}^{(n)} \leftarrow \tilde{g}_{B, \gamma}^{(n-1)} + \frac{1}{n}(r_t - \tilde{g}_{B, \gamma}^{(n-1)})$, where $\tilde{g}_{B, \gamma}^{(0)} = 0$.

The first term of Eq. (3), $1/\tilde{g}_{B, \gamma}$, is mathematically dual to maximizing the amortized throughput. The second term functions as a regularization mechanism for the switching cost. The indicator function $\mathbb{I}(\cdot)$ activates only when the system transitions from a disabled state ($\gamma_{t-1} = 0$) to an enabled state ($\gamma > 0$), incurring a KV cache reconstruction cost c_{prefill} . By dividing this cost by γ , the objective favors configurations that amortize the startup overhead across

longer speculative sequences, thereby discouraging short-sighted switching that degrades system latency.

Algorithm 1 details the execution flow. To handle the asynchronous nature of continuous batching, Nightjar maintains independent state variables for each batch size B , organizing time into a hierarchical structure of *blocks* (indexed by j_B) and *bins* (indexed by b_B).

Initialization and Bin Selection. For every time step t , the algorithm identifies the current batch size B and determines the strategy for the current bin. As shown in Lines 6-8, at the onset of a new bin (when the round counter $\tau_B = 1$), the bin is designated as an *exploration* bin with probability $1/\sqrt{b_B}$ and as an *exploitation* bin otherwise. This decaying exploration probability ensures that the system explores aggressively in the early stages to gather statistics but progressively converges to the optimal policy as the bin index b_B increases.

Execution and State Evolution. During an exploration bin, the speculative length γ_t is sampled uniformly from the available search space to ensure coverage (Lines 9-11). Conversely, in an exploitation bin, the algorithm selects γ_t by solving Eq. (3) to maximize system efficiency (Lines 12-14). Following the execution of γ_t , the system observes the reward $r_t(\gamma_t)$ and updates the internal counters (Line 15).

A key feature of Nightjar is its exponential time scaling. A bin concludes when the round counter τ_B exceeds $\sqrt{H_B}$, and a block concludes when the bin counter b_B exceeds $\sqrt{H_B}$ (Lines 17-22). Upon the completion of a block, the block size is updated via $H_B \leftarrow 2^{j_B-1}$. This exponential growth ensures that as the history length j_B increases, the duration of stable exploitation phases grows significantly, allowing the system to capitalize on refined goodput estimates.

Prefill Cost Modeling The effectiveness of Eq. (3) relies on an accurate estimation of c_{prefill} , which represents the KV cache reconstruction latency. This cost is not static; it varies based on the hardware state and the synchronization gap between the draft and target models. When speculative decoding is re-enabled, the draft model must process all tokens generated by the target model during the inactive period. We quantify this overhead using the *effective skip*

TABLE 3. MEASURED SWITCHING COST (c_{prefill}) ACROSS VARYING BATCH SIZES AND INPUT LENGTHS USING A 7B MODEL ON AN NVIDIA RTX 4090.

Input Length	Batch Size	c_{prefill} (ms)
128	32	17.87
128	64	28.53
256	32	20.65
256	64	22.33
512	32	24.30
512	64	102.03

length, defined as $L_{\max} = \max\{L_1, \dots, L_B\}$, where L_i is the number of new tokens for request i . Since the draft model computes the tokens in parallel, the batch latency is determined by the request with the largest lag. The algorithm queries an offline-populated lookup table $c_{\text{prefill}}(L_{\max}, B)$ (Table 3) to obtain the precise cost. For example, empirical

Algorithm 1: Nightjar Algorithm

Input : Max speculative length Γ_{\max} , Max batch size B_{\max}
Initialize: Global time $t \leftarrow 1$
1 for $B = 1$ **to** B_{\max} **do**
2 | // Initialize per-batch hierarchy states
3 | $j_B \leftarrow 1, H_B \leftarrow 1, b_B \leftarrow 1, \tau_B \leftarrow 1$
4 for *each time step* $t = 1, 2, \dots$ **do**
5 | Receive current batch size $B = B_t$
6 | **if** $\tau_B = 1$ **then**
7 | | // Bin Initialization
8 | | Set bin type: Exploration with prob. $1/\sqrt{b_B}$, else Exploitation
9 | **if** *bin is Exploration* **then**
10 | | // Uniform Exploration
11 | | Sample $\gamma_t \sim \text{Uniform}(\{0, \dots, \Gamma_{\max}\})$
12 | **else**
13 | | // Cost-Aware Exploitation
14 | | Select γ_t via Eq. (3)
15 | Play γ_t , observe reward $r_t(\gamma_t)$ and update $\tilde{g}_{B,\gamma}$
16 | $\tau_B \leftarrow \tau_B + 1$
17 | **if** $\tau_B > \sqrt{H_B}$ **then**
18 | | // Bin Completed
19 | | $b_B \leftarrow b_B + 1, \tau_B \leftarrow 1$
20 | | **if** $b_B > \sqrt{H_B}$ **then**
21 | | | // Block Completed
22 | | | $j_B \leftarrow j_B + 1, H_B \leftarrow 2^{j_B-1}, b_B \leftarrow 1$
23 | $t \leftarrow t + 1$

profiling on a DeepSeek-R1-Distill-Qwen-7B model target model and 0.5B draft model on RTX 4090 indicates that c_{prefill} can range from 17.87 ms to over 102.03 ms depending on L_{\max} , making this dynamic cost retrieval essential for robust decision-making. To construct this lookup table, we performed offline profiling. We measured latencies across a grid of input lengths and geometrically increasing batch sizes (e.g., 2, 4, 8...). Specifically, we recorded the prefill time for the standalone target model (T_{base}) and the prefill time with speculative decoding enabled (T_{SD}). The switching cost c_{prefill} is derived from the difference ($T_{\text{SD}} - T_{\text{base}}$).

Overhead. The arm selection execution time is approximately $1e-5$ seconds, while the average generation time per token in the LLM is 0.034 seconds — a difference of nearly 3400 times. This minimal overhead demonstrates the exceptional efficiency of our method, as the cost of dynamic arm selection is negligible compared to the intrinsic latency of token generation.

4.3. Theoretical Analysis

In this section, we provide a rigorous theoretical analysis for our proposed Nightjar algorithm. We begin by presenting our main theoretical result, Theorem 1, which establishes a sublinear regret bound for the algorithm under the dynamic serving environment. The proof relies on decomposing the

regret into exploration, estimation, and switching cost components.

For the analysis, we assume the goodput reward r_t is bounded in $[0, g_{\max}]$ and the switching cost is bounded by C_{switch} .

4.3.1. Regret of Nightjar. The core element of our proposed framework is the adaptive bin-greedy strategy. The following theorem presents the regret upper bound of Nightjar.

Theorem 1. *For any time horizon T and batch size context B , assuming the switching cost is bounded, there exist positive constants such that with probability at least $1 - \delta$, the cumulative regret of the proposed Nightjar algorithm satisfies:*

$$R(T) \leq \mathcal{O}\left(g_{\max} \sqrt{T \log T} + C_{\text{switch}} \sqrt{T}\right) = \tilde{\mathcal{O}}(\sqrt{T}). \quad (4)$$

Consequently, the average regret satisfies $\lim_{T \rightarrow \infty} R(T)/T = 0$.

Remark 1. *Theorem 1 provides a high-probability theoretical guarantee. Unlike expected regret bounds, this ensures that the algorithm performs efficiently in widely varying single runs, which is critical for system stability in production environments.*

4.3.2. Proof of Theorem 1. To prove Theorem 1, we introduce three supporting lemmas handling estimation confidence, exploration frequency, and switching frequency.

Lemma 1 (Confidence Bound). *For any arm γ and time t , let $N_t(\gamma)$ be the number of times arm γ has been pulled. With probability at least $1 - \delta/2$, the deviation between the empirical mean goodput $\tilde{g}_{t,\gamma}$ and the true mean μ_γ is bounded by the confidence radius $\beta_t(\gamma)$:*

$$|\tilde{g}_{t,\gamma} - \mu_\gamma| \leq \beta_t(\gamma) := \sqrt{\frac{g_{\max}^2 \log(2T/\delta)}{2N_t(\gamma)}}. \quad (5)$$

Lemma 2 (Bounding Exploration). *Under the adaptive binning mechanism, the exploration probability in the b -th bin is set exactly to $p_b = 1/\sqrt{b}$. The cumulative number of exploration steps up to time T is bounded by:*

$$N_{\text{explr}}(T) = \sum_{t=1}^T \mathbb{I}(\text{exploration}_t) \leq \mathcal{O}(\sqrt{T}). \quad (6)$$

Lemma 3 (Bounding Switching Cost). *The total number of speculative length switches, denoted as $S(T)$, is bounded by the sum of exploration switches and exploitation updates. Given the block-bin structure where block size grows geometrically, $S(T)$ satisfies:*

$$S(T) \leq \mathcal{O}(\sqrt{T}). \quad (7)$$

Indeed, switches primarily occur during exploration steps (bounded by Lemma 2) or at bin boundaries; since bin sizes grow with \sqrt{HB} , the frequency of boundary updates decays, which yields $S(T) \leq \mathcal{O}(\sqrt{T})$.

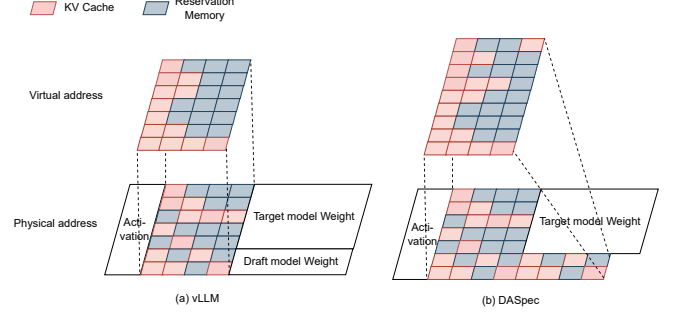


Figure 6. (a) vLLM mitigates memory fragmentation via KV cache virtualization but spatially isolates activation values from the KV cache. (b) Nightjar logically decouples KV cache management from model weights while consolidating them into a unified physical memory pool to maximize utilization.

Based on Lemmas 1, 2, and 3, we derive Theorem 1.

Proof of Theorem 1. The cumulative regret $R(T)$ can be decomposed into three parts: regret from exploration rounds (R_{explr}), regret from suboptimal choices during exploitation due to estimation error (R_{est}), and the cumulative switching cost ($C_{\text{switch}} \cdot S(T)$).

$$\begin{aligned} R(T) &= R_{\text{explr}} + R_{\text{est}} + \text{SwitchingCost}(T) \\ &\leq \underbrace{N_{\text{explr}}(T) \cdot g_{\max}}_{(a)} + \underbrace{\sum_{t \in \mathcal{T}_{\text{exploit}}} (\mu^* - \mu_{\gamma_t})}_{(b)} + \underbrace{S(T) \cdot C_{\text{switch}}}_{(c)} \end{aligned}$$

Term (a): By Lemma 2, the exploration regret is bounded by $g_{\max} \cdot \mathcal{O}(\sqrt{T})$.

Term (c): By Lemma 3, the switching cost is bounded by $C_{\text{switch}} \cdot \mathcal{O}(\sqrt{T})$.

Term (b): For exploitation steps, if a suboptimal arm γ_t is chosen, it implies the empirical estimate \tilde{g}_{t,γ_t} exceeded the optimal \tilde{g}_{t,γ^*} . Using the confidence bound from Lemma 1, the instantaneous regret is bounded by $2\beta_t(\gamma_t)$. Summing over T , standard bandit analysis (deriving from the summation of inverse square roots) yields:

$$\sum_{t=1}^T 2 \sqrt{\frac{g_{\max}^2 \log(2T/\delta)}{2N_t(\gamma_t)}} \leq \mathcal{O}\left(g_{\max} \sqrt{T \log T}\right). \quad (8)$$

Combining these terms:

$$\begin{aligned} R(T) &\leq \mathcal{O}(g_{\max} \sqrt{T}) + \mathcal{O}(g_{\max} \sqrt{T \log T}) + \mathcal{O}(C_{\text{switch}} \sqrt{T}) \\ &= \mathcal{O}\left(\sqrt{T \log T}\right). \end{aligned} \quad (9)$$

This completes the proof. \square

5. Elastic Memory Management for Model-Based Draft Models

Under high system contention, characterized by a backlog in the request queue, the scarcity of KV cache memory

often necessitates frequent swap operations or the rejection of active requests. In such saturation regimes, speculative decoding becomes counter-productive due to scheduling overheads. To address this, we propose a dynamic offloading mechanism for model-based draft models. As illustrated in Figure 6, we offload the draft model weights—analogueous to LoRA adapter management—to the host memory, thereby reclaiming GPU memory to expand the capacity of the original KV cache. Let M_{orig} denote the baseline KV cache capacity; the expanded capacity is defined as $M_{\text{scale}} = M_{\text{orig}} + S_{\text{draft}}$, where S_{draft} represents the memory footprint of the draft model.

5.1. Trigger Conditions for Dynamic Adjustment

The system employs an elasticity policy based on real-time metrics of KV cache occupancy and queue depth. A **KV cache expansion** event is triggered when the following conditions converge: (1) Speculative decoding is disabled; (2) The number of available memory blocks, denoted as N_{free} , falls below a critical threshold τ_{low} ($N_{\text{free}} < \tau_{\text{low}}$); (3) This resource scarcity persists for a temporal window of T_{persist} scheduling steps.

Conversely, a **KV cache contraction** is initiated to restore the draft model when: (1) The waiting queue is empty ($|Q_{\text{wait}}| = 0$); (2) Sufficient memory exists to accommodate both the draft model and a safety buffer ($N_{\text{free}} > S_{\text{draft}} + \tau_{\text{low}}$). This hysteresis design ensures that speculative decoding remains disabled during high-load phases (where $N_{\text{free}} < \tau_{\text{low}}$), thereby preventing resource thrashing.

5.2. Mechanism of KV Cache Expansion

Upon triggering expansion, the system dynamically re-allocates GPU memory. The Model Executor allocates a contiguous memory segment of size S_{draft} to the KV cache pool. Subsequently, the Block Manager updates its internal state: (1) The set of allocatable physical block indices is expanded to include the new range $[K_{\text{curr}}, K_{\text{new}}]$; (2) Reference counters for these newly instantiated blocks are initialized to zero; (3) The new block indices are appended to the free block queue. Crucially, this process is implemented via in-place expansion, eliminating the need for massive memory copying and minimizing reconfiguration overhead.

5.3. KV Cache Contraction and Logical Remapping

Contraction is the most critical phase, requiring the compaction of the physical memory layout without compromising active contexts. As depicted in Figure 7, the process involves four sequential steps:

Step 1: Identification of Eviction Candidates. The system scans the page tables of all active sequences to identify the set of physical blocks $\mathcal{B}_{\text{evict}}$ located in the memory region to be reclaimed (i.e., blocks with $\text{ID} \geq K_{\text{new}}$). These blocks must be migrated to the preserved memory region $[0, K_{\text{new}}]$.

Step 2: Construction of Migration Plan. We verify available slots in the free list with IDs strictly less than K_{new} . A mapping $\mathcal{M} : b_{\text{old}} \rightarrow b_{\text{new}}$ is constructed. To preserve logical dependencies (specifically, the pointers to predecessor blocks), we apply a topological sort to the migration set. This ensures that blocks are migrated in an order that maintains the integrity of the dependency chain.

Step 3: Metadata Update and Remapping. For each block requiring migration, the system performs atomic metadata updates: (a) A new physical block object is instantiated, inheriting the token sequence and size of the original; (b) Predecessor pointers are updated—if a predecessor block is also part of the migration set, the pointer is redirected to its new location; otherwise, the original reference is maintained; (c) The logical Block Table is updated to map the sequence to the new physical block ID; (d) The reference counter for the new block is incremented, and it is marked as allocated. Finally, the old physical block is released, ensuring the logical sequence remains consistent with the physical memory state.

Step 4: Vectorized Data Migration. Following the metadata update, the physical data transfer is executed. To handle potential circular dependencies in the mapping (e.g., $A \rightarrow B$ and $B \rightarrow A$), the topological sort resolves execution order, isolating any simplified cyclic swaps. The migration is powered by a custom high-performance kernel (implemented in Triton) utilizing a tile-based parallelization strategy. Each thread block manages the transfer of a complete KV cache block via vectorized load/store instructions. This approach provides robust performance even on hardware lacking advanced virtual memory management (VMM) features like `cuMemMap`. By decoupling memory reclamation from model execution, we eliminate deadlock risks associated with "hold-and-wait" patterns.

Step 5: Allocator State Finalization. Post-migration, the block allocator trims its index set, removing $\text{IDs} \geq K_{\text{new}}$ and clearing associated reference counts, effectively finalizing the contraction.

5.4. Non-blocking Asynchronous Migration

To minimize latency, we leverage the fact that speculative decoding is inactive during the unloading phase. Consequently, draft model weights are evicted from the GPU immediately, with a backup retained in host memory. Conversely, when VRAM availability indicates a low request rate, the draft model is reloaded to resume accelerated generation. This reloading process utilizes asynchronous CUDA streams with non-blocking Direct Memory Access (DMA). This allows data transfer to overlap with ongoing computation, ensuring that the background management of model weights incurs negligible impact on the serving latency of the primary model.

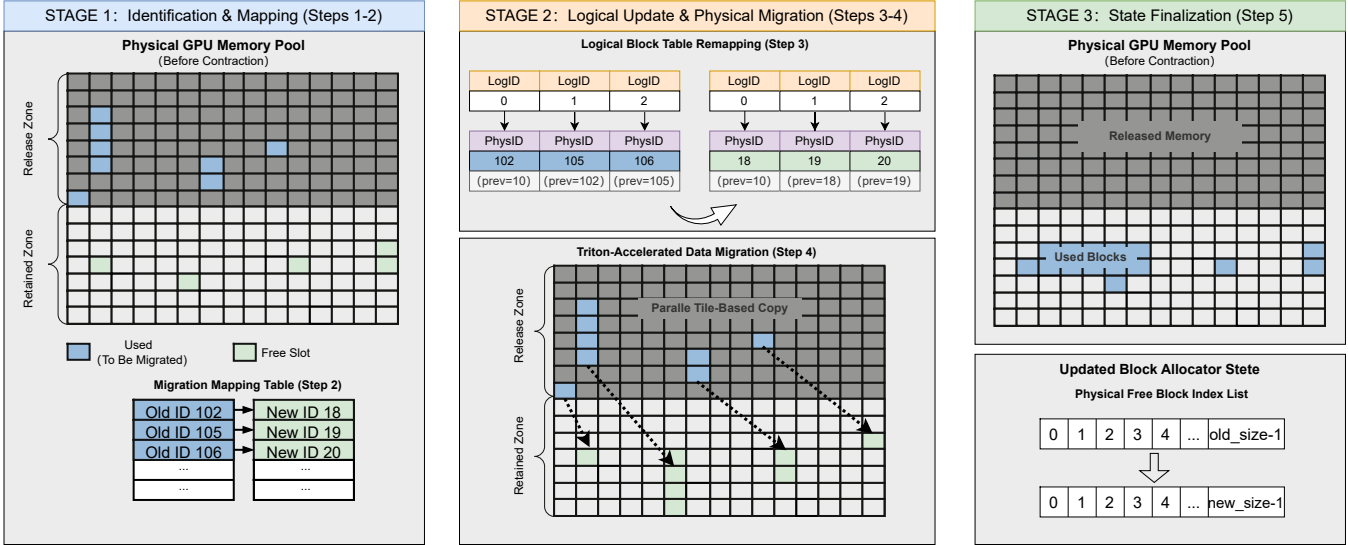


Figure 7. Overview of the KV Cache Block Contraction and Logical Table Remapping process. The system ensures data consistency during physical memory compaction through topological sorting and vectorized data migration.

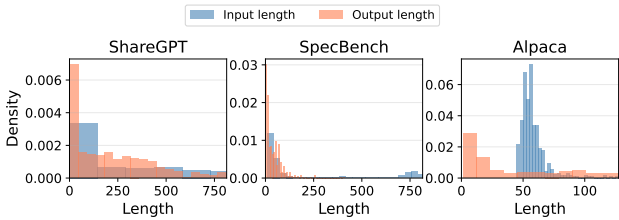


Figure 8. Distribution of Input and Output Lengths Across Three Datasets.

6. Experiments

6.1. Experiment setup

Settings. We select DeepSeek-R1-Distill-Qwen-7B [26] and Vicuna-13b [27] as target models and match them with DeepSeek-R1-DRAFT-Qwen2.5-0.5B [19] and vicuna-68m [28] as draft models respectively. The model pair for the 7B target model is operated on a single RTX 4090 (24GB) GPU, and the model pair for the 13B target model operates on an A100 (40GB) GPU. Nightjar is implemented by extending the vLLM (version 0.8.2) [4].

Workloads. To simulate a dynamic user environment, we generate request arrivals using a Poisson distribution. We also selected real-world production traces from the AzureLLMInferenceDataset [29], and chose a segment with dynamic request rates as shown in Figure 10. For online chatting, we utilize datasets from ShareGPT [30], Alpaca [31]. For other tasks, we utilize SpecBench [1], which is composed of 480 randomly selected instances from six widely used databases. For each dataset, we use 480 instances. The input and output length distribution is presented in Figure 8.

Baselines. We evaluate the total token throughput (tokens/s) and mean end-to-end latency of Nightjar against baseline methods:

- **Standard Speculative Decoding (SD):** Implemented on top of vLLM, this baseline employs a vanilla chain-style draft generation (e.g., $\gamma = 3$), where the draft model generates a sequence of candidate tokens followed by parallel verification from the target model.
- **Vanilla Decoding (w/o SD):** This baseline does not use speculative decoding, where the target model directly generates the response tokens without using the draft model.
- **Dynamic Speculative Decoding (DSD) [13]:** This method utilizes a linear regression model to predict execution latency and estimates the expected acceptance rate based on historical statistics. It dynamically selects the speculative length that maximizes the system *goodput*, defined as the ratio of the expected number of accepted tokens (accepted length + 1) to the execution time.
- **BanditSpec [12]:** This approach treats the selection of speculative length as a Multi-Armed Bandit (MAB) problem, leveraging a variant of the Upper Confidence Bound (UCB) algorithm for optimization. However, it does not explicitly incorporate batch size as a contextual feature in its decision-making process.
- **TETRIS [16]:** Given a fixed speculative length (similar to standard SD), TETRIS keeps the draft generation process intact but re-engineers the verification phase. Within a predefined computational budget, it prioritizes the verification of tokens with the highest predictive entropy across a batch to improve verifi-

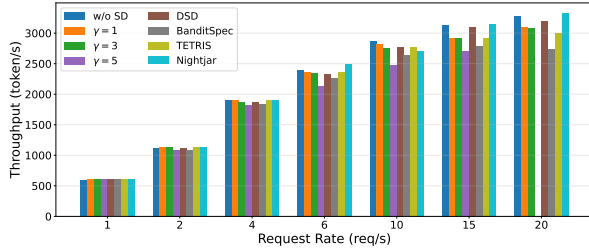


Figure 9. Method Comparison at Low Request Rate and High Request Rate for 7B model.

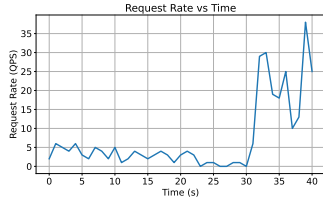


Figure 10. Request Rate Trace.

ation efficiency.

Our result is averaged over 5 independent runs.

Nightjar demonstrates robust performance across varying load conditions by dynamically adapting its speculation strategy. As shown in Figure 9, in the detailed breakdown by request rate on ShareGPT dataset, under low request rates (Request Rate ≤ 4) where speculative decoding outperforms standard decoding, Nightjar maximizes efficiency by selecting the optimal draft length. Conversely, in high request rate scenarios where the overhead of SD renders it inferior to the baseline, Nightjar adaptively disables speculation to avoid performance degradation, thereby consistently achieving superior results in both regimes. Note that data for $\gamma = 5$ at 20 QPS is excluded from Figure 9 owing to GPU memory limitations.

6.2. Dynamic request load

For 7B model under dynamic request rate (Figure 10), as shown in Figure 11, Nightjar surges ahead during low request load periods, achieving the highest peak throughput (3800 tokens/s) and maintaining a consistent lead over rivals during high load phases. DSD’s predictions are less accurate during low request load, leading to throughput degradation, but perform better under high request load, while TETRIS exhibits performance drops under high request load due to its high overhead in large batch size and static BanditSpec is not suitable for dynamic batch size.

As shown in Table 4, Nightjar consistently achieves the highest throughput, demonstrating superior scalability over both static and dynamic baselines. While SD provides moderate gains, Nightjar significantly amplifies these benefits. Notably, on the 13B model, Nightjar achieves a remarkable 64.6% improvement over vanilla decoding (w/o SD) on the Alpaca dataset. More importantly, Nightjar shows

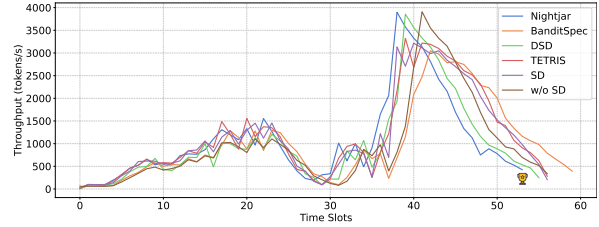


Figure 11. Throughput Trace for 7B model under dynamic request rate.

TABLE 4. THROUGHPUT (TOKENS/S) COMPARISON FOR 7B AND 13B MODELS

Method	7B			13B		
	Alpaca	ShareGPT	SpecBench	Alpaca	ShareGPT	SpecBench
Nightjar	2102.73	3734.23	3326.20	721.23	1729.68	1061.82
BanditSpec	1860.74	3428.75	2631.43	679.82	1383.81	763.15
DSD	2044.40	3614.65	2789.51	603.32	1244.96	692.01
TETRIS	1875.91	3597.21	2974.14	702.65	1628.86	985.40
SD	1920.63	3593.36	3044.80	628.47	1689.53	964.02
w/o SD	2072.38	3653.61	3207.28	438.13	1290.04	673.48

exceptional robustness in complex scenarios. Compared to the advanced inference system TETRIS, Nightjar maintains a consistent lead, achieving a 12.1% throughput gain on the 7B Alpaca dataset. Furthermore, on the 13B SpecBench dataset, Nightjar outperforms the competing DSD method by a substantial 53.4% and BanditSpec by 39.1%. Even against the optimized fixed-length SD baseline, Nightjar maintains a clear advantage, proving that its cost-aware policy effectively identifies optimal lengths.

Regarding end-to-end latency, Table 5 further validates Nightjar’s efficiency. For the 7B model, Nightjar reduces latency by 20.2% compared to SD on the Alpaca dataset. Crucially, Nightjar demonstrates superior lightweight scheduling compared to TETRIS. On the 7B Alpaca dataset, Nightjar reduces latency by 24.4% compared to TETRIS, indicating that Nightjar effectively mitigates the complex sampling overheads that hinder TETRIS. On the 13B model, the advantage remains significant against other dynamic baselines: Nightjar reduces latency by 34.3% compared to DSD on SpecBench. This confirms that Nightjar’s bandit-based mechanism avoids the “decision deadlock” and high penalty costs that hamper DSD in high-load, compute-bound environments.

6.3. Ablation and Analysis

6.3.1. Context-Aware Bandit Methods. We conduct ablation experiments on 7B model. Figure 12 additionally compares various context-aware multi-armed bandit methods (batch size as context) and the basic ADA-BINGREEDY

TABLE 5. MEAN END-TO-END LATENCY (MS) COMPARISON FOR 7B AND 13B MODELS

Method	7B			13B		
	Alpaca	ShareGPT	SpecBench	Alpaca	ShareGPT	SpecBench
Nightjar	8868.17	6534.76	7618.85	23525.49	8133.92	14691.81
BanditSpec	12340.83	7799.63	9288.23	29077.32	9667.04	19294.42
DSD	9183.21	6499.12	8301.02	16212.44	10057.72	22361.71
TETRIS	11734.19	7409.62	8789.48	22133.43	8046.25	14937.37
SD	11110.68	7047.49	8567.04	24671.40	8152.97	14212.97
w/o SD	8876.14	6438.47	7654.05	32222.49	9350.87	23831.74

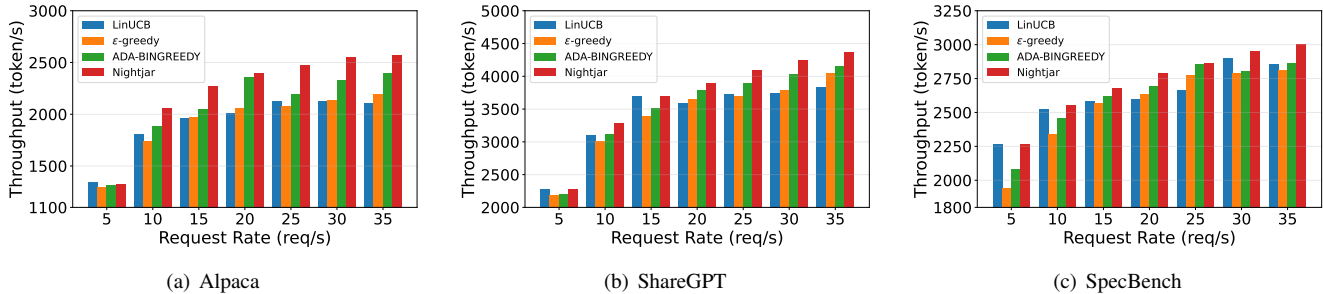


Figure 12. Context-aware bandit method comparison on Alpaca, ShareGPT and SpecBench datasets.

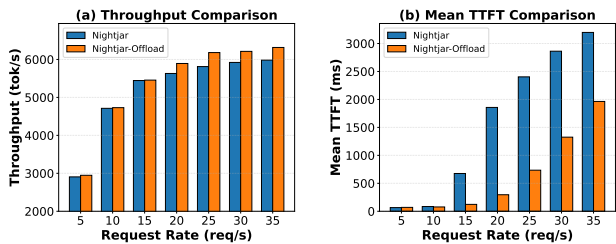


Figure 13. Performance Comparison of with offload and without offload

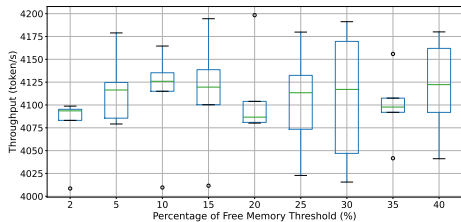


Figure 14. Performance Comparison of with different thresholds

approach. Our method consistently achieves optimal performance across different QPS levels because LinUCB and linearTS assume linear relationships between rewards and contexts, which don't hold for LLM speculative serving scenarios. Throughput depends not only on hardware but also on acceptance rates and model types, making linear models unsuitable for this complex scenario.

6.3.2. Efficacy of Dynamic Model Offloading. The impact of our dynamic loading and unloading mechanism is assessed by comparing Nightjar-Offload with the standard Nightjar implementation. Results in Figure 13 demonstrate that offloading becomes increasingly beneficial as the system enters the compute-bound regime at high request rates, reaching a peak throughput of 6315.9 tok/s at 35 req/s—a substantial improvement over the 5982.6 tok/s achieved without offloading. This confirms that liberating GPU memory by unloading draft models effectively expands the KV cache capacity for the target model, directly translating to higher service concurrency.

6.3.3. Sensitivity to Trigger Thresholds. We further investigate the sensitivity of system performance to the free

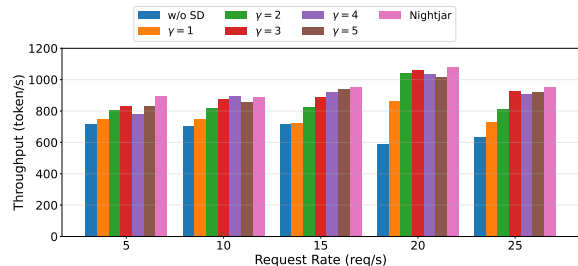


Figure 15. Throughput comparison for static request rate on SpecBench dataset. Comparison among different speculative length γ for 13B model.

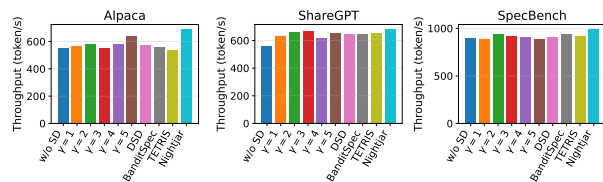


Figure 16. Performance Comparison of 30B model

KV cache threshold N_{low} , which dictates the timing for dynamic adjustments. Figure 14 illustrates that the system reaches an optimal throughput plateau of approximately 6110 tok/s at a 10% free cache threshold, which significantly exceeds the fixed baseline performance of 5768.12 tok/s. This result indicates that a 10% buffer provides the ideal balance between sustaining speculative decoding and preventing memory exhaustion, ensuring robust QoS under heavy traffic conditions.

6.3.4. Compare with different speculative length. As shown in Figure 15, when compared against the best-performing fixed speculative lengths (such as $\gamma = 2$ or $\gamma = 4$ at their peak efficiency) for 13B model, Nightjar consistently maintains a 1% to 16% performance advantage. This demonstrates exceptional robustness, as Nightjar never falls behind the optimal static configuration.

6.3.5. Scalability Analysis on Multi-GPU Settings. In this experiment, we deploy a 30B-scale model across two NVIDIA L20 (48GB) GPUs using tensor parallelism. Specifically, we use Qwen2.5-32B-Instruct as the target

model and Qwen2.5-0.5B-Instruct as the draft model. As shown in Figure 16, by comparing Nightjar against other baselines, we observe that Nightjar maintains its performance advantage even when scaling to larger models distributed across multiple GPUs.

TABLE 6. OVERHEAD OF ELASTIC MEMORY OPERATIONS FOR 30B MODEL ON 2 L20 GPUS.

Operation	Latency
KV Cache Block Expansion	143.9 ms
KV Cache Block Contraction (Triton-accelerated)	11.9 ms
Draft Model Reload Dispatch (CPU Overhead)	21.9 μ s

6.3.6. Overhead of Elastic Memory Operations. As shown in Table 6, we further quantified the overhead of these dynamic adjustments to ensure they do not disrupt real-time serving for 30B model on 2 L20 GPUs. The KV cache contraction process, accelerated by our custom Triton kernel, completes in just 11.9 ms, allowing for rapid memory reclamation during load spikes. Conversely, KV cache expansion takes 143.9 ms, a simplified cost acceptable during the transition to low-load states. Notably, triggering the draft model reload incurs a negligible CPU overhead of only 21.9 μ s, confirming that our non-blocking asynchronous stream management effectively hides the data transfer latency from the critical scheduling path.

7. Related Work

7.1. Speculative Decoding in LLM Serving

While various approaches have sought to optimize speculative decoding, they often fail to address the dynamic and unpredictable nature of real-world LLM serving loads. Initial efforts focused on single-request optimization [6], [7], [8], [9], [10] or static offline batches [11], [12], employing predictive algorithms [7] or confidence-based methods [14], [6], [16], but their static nature makes them fundamentally ill-suited for the fluctuating request rates in live environments. More recent works have explored dynamic speculation length adjustment in serving systems [11], [13], [14], [15], yet they exhibit significant limitations. For instance, SpecServe [14] and TETRIS [16] rely on draft confidence scores, but this can lead to poor performance with large batch sizes and still requires generating at least one token. DSD [13] optimizes length via linear goodput modeling, but its reliance on past average acceptance rates introduces a critical vulnerability. This dependency on historical data, found in methods like DSD [13] and SpecServe [14], can lead to a “decision deadlock” where disabling speculative decoding permanently halts the collection of new acceptance rate data, locking the system in a suboptimal state. Our exploration-exploitation approach is designed to mitigate this risk. Even the work of BanditSpec [12], which first introduced a Multi-Armed Bandit (MAB) paradigm, is constrained by its static design, rendering it incompatible with

the continuous batching [4] of modern serving systems. Furthermore, to the best of our knowledge, existing works largely overlook the “switching cost” incurred when re-enabling speculative decoding from a length of 0, which is the overhead of KV cache reconstruction for the draft model.

7.2. Unified Memory Management for Weights and KV Cache in LLM Serving

Oneiros [17] targets multi-model deployment by introducing a dynamic memory remapping engine that redirects GPU memory reserved for model parameters to the KV cache. Unlike Nightjar, which completely unloads draft model weights when they are not in use, Oneiros operates on active models. By performing remapping at layer granularity, it enables models to remain in a serving state while utilizing asynchronous transfers to fetch required parameters in real-time before execution. This approach effectively hides latency by overlapping computation with parameter transfer. eLLM [18] focuses on intra-model efficiency, enabling the KV cache and activation tensors to “borrow” space from a shared physical memory pool, effectively breaking the traditional isolation between these resources. FineServe [32] provides a unified management framework for both weights and KV caches across multiple models, specifically addressing the challenges of serving models with heterogeneous quantization precisions.

8. Conclusions

In this paper, we presented Nightjar, an innovative learning-based algorithm for optimizing speculative decoding. By modeling the speculative length selection as a multi-armed bandit problem, Nightjar dynamically chooses the best decoding strategy for different batch sizes, maximizing throughput and minimizing latency. Extensive evaluations confirm that Nightjar provides superior performance, highlighting a promising direction for more efficient and responsive LLM serving solutions.

References

- [1] H. Xia, Z. Yang, Q. Dong, P. Wang, Y. Li, T. Ge, T. Liu, W. Li, and Z. Sui, “Unlocking efficiency in large language model inference: A comprehensive survey of speculative decoding,” in *Findings of the Association for Computational Linguistics ACL 2024*, Aug. 2024, pp. 7655–7671.
- [2] Y. Leviathan, M. Kalman, and Y. Matias, “Fast inference from transformers via speculative decoding,” in *International Conference on Machine Learning*. PMLR, 2023, pp. 19 274–19 286.
- [3] L. Zhang, Z. Zhang, R. Li, Z. Tian, S. Mei, D. Li *et al.*, “Dovetail: A cpu/gpu heterogeneous speculative decoding for llm inference,” in *Proceedings of the 2025 Conference on Empirical Methods in Natural Language Processing*, 2025, pp. 17 393–17 406.
- [4] W. Kwon, Z. Li, S. Zhuang, Y. Sheng, L. Zheng, C. H. Yu, J. Gonzalez, H. Zhang, and I. Stoica, “Efficient memory management for large language model serving with pagedattention,” in *Proceedings of the 29th symposium on operating systems principles*, 2023, pp. 611–626.

- [5] X. Liu, J. Yu, J. Park, I. Stoica, and A. Cheung, "Speculative decoding: Performance or illusion?" *arXiv preprint arXiv:2601.11580*, 2025.
- [6] J. Wang, Y. Su, J. Li, Q. Xia, Z. Ye, X. Duan, Z. Wang, and M. Zhang, "Opt-tree: Speculative decoding with adaptive draft tree structure," *Transactions of the Association for Computational Linguistics*, vol. 13, pp. 188–199, 2025.
- [7] S. Zhang, H. Wang, D. Ma, Z. Zhu, L. Chen, K. Lan, and K. Yu, "Adaegle: Optimizing speculative decoding via explicit modeling of adaptive draft structures," *arXiv preprint arXiv:2412.18910*, 2024.
- [8] Z. Zhang, J. Xu, T. Liang, X. Chen, Z. He, R. Wang, and Z. Tu, "Draft model knows when to stop: A self-verification length policy for speculative decoding," *arXiv preprint arXiv:2411.18462*, 2024.
- [9] O. Brown, Z. Wang, A. Do, N. Mathew, and C. Yu, "Dynamic depth decoding: Faster speculative decoding for llms," *arXiv preprint arXiv:2409.00142*, 2024.
- [10] K. Huang, X. Guo, and M. Wang, "Specdec++: Boosting speculative decoding via adaptive candidate lengths," *arXiv preprint arXiv:2405.19715*, 2024.
- [11] Q. Su, C. Giannoula, and G. Pekhimenko, "The synergy of speculative decoding and batching in serving large language models," *arXiv preprint arXiv:2310.18813*, 2023.
- [12] Y. Hou, F. Zhang, C. Du, X. Zhang, J. Pan, T. Pang, C. Du, V. Y. Tan, and Z. Yang, "Banditspec: Adaptive speculative decoding via bandit algorithms," *arXiv preprint arXiv:2505.15141*, 2025.
- [13] X. Liu, C. Daniel, L. Hu, W. Kwon, Z. Li, X. Mo, A. Cheung, Z. Deng, I. Stoica, and H. Zhang, "Optimizing speculative decoding for serving large language models using goodput," *arXiv preprint arXiv:2406.14066*, 2024.
- [14] K. Huang, H. Wu, Z. Shi, H. Zou, M. Yu, and Q. Shi, "Specserve: Efficient and slo-aware large language model serving with adaptive speculative decoding," *arXiv preprint arXiv:2503.05096*, 2025.
- [15] Z. Li, Z. Chen, R. Delacourt, G. Oliaro, Z. Wang, Q. Chen, S. Lin, A. Yang, Z. Zhang, Z. Chen *et al.*, "Adaserve: Slo-customized llm serving with fine-grained speculative decoding," *arXiv e-prints*, pp. arXiv-2501, 2025.
- [16] Z. Wu, Z. Zhou, A. Verma, A. Prakash, D. Rus, and B. K. H. Low, "Tetris: Optimal draft token selection for batch speculative decoding," *arXiv preprint arXiv:2502.15197*, 2025.
- [17] R. Li, S. Pal, V. N. Pullu, P. Sinha, J. Ryoo, L. K. John, and N. J. Yadwadkar, "Oneiros: Kv cache optimization through parameter remapping for multi-tenant llm serving," in *Proceedings of the 2025 ACM Symposium on Cloud Computing*, 2025, pp. 88–101.
- [18] J. Xu, R. Zhang, Y. Xiong, C. Guo, Z. Liu, Y. Zhou, W. Hu, H. Wu, C. Shao, Z. Wang *et al.*, "ellm: Elastic memory management framework for efficient llm serving," *arXiv preprint arXiv:2506.15155*, 2025.
- [19] Alamos, "Deepseek-r1-draft-qwen2.5-0.5b," <https://huggingface.co/alamios/DeepSeek-R1-DRAFT-Qwen2.5-0.5B>, 2024, accessed: 2025-03-30.
- [20] R. Sadhukhan, J. Chen, Z. Chen, V. Tiwari, R. Lai, J. Shi, I. E.-H. Yen, A. May, T. Chen, and B. Chen, "Magicdec: Breaking the latency-throughput tradeoff for long context generation with speculative decoding," *arXiv preprint arXiv:2408.11049*, 2024.
- [21] D. Guo, D. Yang, H. Zhang, J. Song, R. Zhang, R. Xu, Q. Zhu, S. Ma, P. Wang, X. Bi *et al.*, "Deepseek-r1: Incentivizing reasoning capability in llms via reinforcement learning," *arXiv preprint arXiv:2501.12948*, 2025.
- [22] S. Agrawal and N. Goyal, "Thompson sampling for contextual bandits with linear payoffs," in *International conference on machine learning*. PMLR, 2013, pp. 127–135.
- [23] L. Li, W. Chu, J. Langford, and R. E. Schapire, "A contextual-bandit approach to personalized news article recommendation," in *Proceedings of the 19th international conference on World wide web*, 2010, pp. 661–670.
- [24] A. Stolcke, A. Raju, C. Vaz, D. He, V. Ravichandran, V. A. Trinh *et al.*, "Adaptive endpointing with deep contextual multi-armed bandits," in *ICASSP 2023-2023 IEEE International Conference on Acoustics, Speech and Signal Processing (ICASSP)*. IEEE, 2023, pp. 1–5.
- [25] H. Luo, C.-Y. Wei, A. Agarwal, and J. Langford, "Efficient contextual bandits in non-stationary worlds," in *Conference On Learning Theory*. PMLR, 2018, pp. 1739–1776.
- [26] DeepSeek, "Deepseek-r1-distill-qwen-7b," <https://huggingface.co/deepseek-ai/DeepSeek-R1-Distill-Qwen-7B>, 2024, accessed: 2025-03-20.
- [27] lmsys, "vicuna-13b-v1.5," Hugging Face Model Hub, accessed: 2025-08-14. [Online]. Available: <https://huggingface.co/lmsys/vicuna-13b-v1.5>
- [28] double7, "vicuna-68m," Hugging Face Model Hub, accessed: 2025-08-14. [Online]. Available: <https://huggingface.co/double7/vicuna-68m>
- [29] M. Azure, "Azure public dataset," <https://github.com/Azure/AzurePublicDataset>, 2023, accessed: 2025-03-20.
- [30] anon8231489123, "Sharegpt_v3_unfiltered_cleaned_split_no_imsorry.json," https://huggingface.co/datasets/anon8231489123/ShareGPT_Vicuna_unfiltered/blob/main/ShareGPT_V3_unfiltered_cleaned_split_no_imsorry.json, 2023, accessed: 2025-03-20.
- [31] T. Lab, "Alpaca dataset," <https://huggingface.co/datasets/tatsu-lab/alpaca>, 2023, accessed: 2025-04-15.
- [32] K. Bin, S. Choi, J. Son, J. Choi, D. Bae, D. Baek, K. Moon, M. Jang, and H. Lee, "Fineserve: Precision-aware kv slab and two-level scheduling for heterogeneous precision llm serving," *arXiv preprint arXiv:2509.06261*, 2025.